

Imaging for deep brain stimulation: The zona incerta at 7 Tesla

Hans U Kerl, Lars Gerigk, Marc A Brockmann, Sonia Huck, Mansour Al-Zghloul, Christoph Groden, Thomas Hauser, Armin M Nagel, Ingo S Nölte

Hans U Kerl, Marc A Brockmann, Sonia Huck, Mansour Al-Zghloul, Christoph Groden, Ingo S Nölte, Department of Neuroradiology, University Medical Center Mannheim, University of Heidelberg, 68167 Mannheim, Germany

Lars Gerigk, Thomas Hauser, Division of Radiology, German Cancer Research Center, 69120 Heidelberg, Germany

Armin M Nagel, Department of Medical Physics and Radiology, German Cancer Research Center, 69120 Heidelberg, Germany

Author contributions: Kerl HU and Gerigk L contributed equally to this work; Kerl HU, Gerigk L and Nölte IS designed the study; Gerigk L, Hauser T and Nagel AM were responsible for the acquisition of the scans; Brockmann MA, Huck S, Al-Zghoul M and Groden C edited the manuscript; Kerl HU and Nölte IS wrote the paper; all authors contributed to supportive work.

Correspondence to: Dr. Ingo S Nölte, MED, Department of Neuroradiology, University Medical Center Mannheim, University of Heidelberg, Theodor-Kutzer-Ufer 1-3, 68167 Mannheim, Germany. ingo.noelte@umm.de

Telephone: +49-621-3832443 Fax: +49-621-3832165

Received: September 20, 2012 Revised: October 24, 2012

Accepted: January 17, 2013

Published online: January 28, 2013

images were co-registered with a stereotactic atlas (Schaltenbrand-Wahren).

RESULTS: The rostral part of the ZI (rZI) could easily be identified and was best and reliably visualized in the coronal FLASH2D-T2Star images. The caudal part was not definable in any of the sequences. No major artifacts in the rZI were observed in any of the scans. FLASH2D-T2Star and SWI imaging offered significant higher CNR values for the rZI compared to T2-TSE images ($P > 0.05$). The co-registration of the coronal FLASH2D-T2Star images with the stereotactic atlas schema (Schaltenbrand-Wahren) confirmed the correct localization of the ZI in all cases.

CONCLUSION: FLASH2D-T2Star imaging (particularly coronal view) provides the reliable and currently optimal visualization of the rZI at 7.0 T. These results can facilitate a better and more precise targeting of the caudal part of the ZI than ever before.

© 2013 Baishideng. All rights reserved.

Abstract

AIM: To evaluate different promising magnetic resonance imaging (MRI) methods at 7.0 Tesla (T) for the pre-stereotactic visualization of the zona incerta (ZI).

METHODS: Two neuroradiologists qualitatively and quantitatively examined T2-turbo spin-echo (T2-TSE), T1-weighted gradient-echo, as well as FLASH2D-T2Star and susceptibility-weighted imaging (SWI) for the visualization of the ZI at 7.0 T MRI. Delineation and image quality for the ZI were independently examined using a 6-scale grading system. Inter-rater reliability using Cohen's kappa coefficient (κ) were assessed. Contrast-to-noise ratios (CNR), and signal-to-noise ratios (SNR) for the ZI were calculated for all sequences. Differences in delineation, SNR, and CNR between the sequences were statistically assessed using a paired *t*-test. For the anatomic validation the coronal FLASH2D-T2Star

Key words: Deep brain stimulation; Essential tremor; Magnetic resonance imaging; Parkinson's disease; Zona incerta; 7 Tesla

Kerl HU, Gerigk L, Brockmann MA, Huck S, Al-Zghloul M, Groden C, Hauser T, Nagel AM, Nölte IS. Imaging for deep brain stimulation: The zona incerta at 7 Tesla. *World J Radiol* 2013; 5(1): 5-16 Available from: URL: <http://www.wjgnet.com/1949-8470/full/v5/i1/5.htm> DOI: <http://dx.doi.org/10.4329/wjr.v5.i1.5>

INTRODUCTION

Deep brain stimulation (DBS) is an accepted neurosurgical technique for the treatment of many neurological and psychiatric disorders, such as Parkinson's disease (PD), essential tremor (ET), dystonia^[1-4]. The subthalam-

ic nucleus (STN) represents the commonly chosen target site to suppress resting tremor in patients with PD^[1,5,6]. Despite the improvements in motor function, several clinical trials have yielded information about negative limbic effects of STN DBS, including depression, apathy, and decreased cognitive function^[7,8].

Recent studies, however, have reported that the most effective contact of a quadripolar DBS lead (contact 3 in DBS of the STN) lies dorsal/dorsomedial to the STN, in the region of the zona incerta (ZI)^[9-11].

The ZI, an embryological derivate of the ventral thalamus, is a small horizontally elongated area of grey matter cells in the subthalamic region of the mesencephalon. The nucleus gains increasing importance as an alternative target for the treatment with DBS of various neurological and psychiatric disorders including ET and PD^[12,13]. It is located at the base of the dorsal thalamus and separates the lenticular fasciculus from the thalamic fasciculus ("field H1 and H2 of Forel")^[14,15]. The nucleus is a distinct heterogeneous structure with up to 20 different types of neurochemically defined cells^[16]. Functionally the ZI is divided into two main parts (rostral and caudal). Each is thought to have several physiological functions: The rostral component (rZI), attributed to the visceral control^[17], extends over the dorsal and medial surface of the STN separated by the pallidofugal fibres (PFF) and crossing the internal capsule (Ci). The caudal part (cZI) or the motor component is located posteromedial to the STN and extends behind the prelemniscal radiation^[18]. Ventrocaudally to the ZI lies the substantia nigra^[19,20], laterally the Ci, and dorsomedially the red nucleus^[21,22].

A recent study by Burrows *et al.*^[23] comparing DBS of the STN and the ZI provided similar findings resulting in sustained motor benefit with less limbic side effects, including anxiety and self-reported depression, for ZI stimulation. Furthermore, the stimulation of the cZI^[18,24,25] seems to be superior compared to the stimulation of the STN in improving contralateral parkinsonism^[26]. Moreover, a prospective study suggested that bilateral stimulation of the cZI nucleus is effective in suppressing tremors of various etiologies of both the distal and proximal extremities^[25].

Previous studies including magnetic resonance imaging (MRI) studies up to 1.5 T showed that the visualization of the ZI is unsatisfactory as the small nucleus is hard to distinguish from the surrounding vital structures in the subthalamic region^[27,28]. Therefore, different indirect targeting approaches have been established. These indirect techniques use proportional calculation schemata, relative to a line connecting the anterior and posterior commissures and other more closely located landmarks as the red nucleus and the STN [measured by ventriculography, computed tomography (CT) or MRI], estimating the position of the target structure by empirical values^[29-31]. Similarly, atlas-derived maps co-registered to the magnetic resonance images are used to more accurately delimit the localization of the target area^[31,32]. Apart

from pre-operative imaging, intra-operative electrophysiological function mapping is used to confirm the exact stereotactic position^[33,34].

In contrast, the direct targeting method employs stereotactic pre-operative MRI for the visualization and localization of the target structure. As the subthalamic region varies considerably in position and size^[35,36], the individually optimal electrode position can be achieved.

Lately published studies of 7.0 T MRI for deep brain structures provided initial promising results due to an increase in tissue contrast compared to lower field strengths^[27,37]. Besides the most frequently used heavily T2-weighted fast spin-echo^[20,31,38] new sequences including quantitative T1 and T2 imaging^[39,40], T2* mapping^[41-43] and susceptibility-weighted imaging (SWI)^[44], have been proposed to improve the visibility of the target structures. For the ZI no respective data exists. The aim of this study is to compare different promising MRI methods at 7.0 T (sequence and orientation) for the direct visualization of the ZI.

MATERIALS AND METHODS

Participant characteristics

Nine healthy volunteers (five male, four female) with a mean age of twenty-five years (range 21-28 years) were enrolled in this study.

Informed consent was obtained from all participants. The study was approved by the local research ethics committee. The approval also covers the analysis of other brain regions of the volunteers not addressed in this study.

MRI

For MR imaging of all subjects a whole body 7.0 T MRI system (Magnetom, Siemens Healthcare, Erlangen, Germany) with a 24 channel receive and single channel transmit head coil (Nova Medical, Wilmington, MA, United States) was used. The following sequences were acquired: T2-turbo spin-echo (T2-TSE), T1-weighted gradient-echo (T1-GRE), T2-star-weighted two-dimensional fast low angle shot MRI (FLASH2D-T2Star) and SWI. The specific imaging parameters used are summarized in Table 1.

Slice thickness was manually adapted to completely cover the area of interest while maintaining an adequate acquisition time. Axial and coronal views of the isotropic T1-GRE were reconstructed in-plane with a slice thickness of 0.51 mm. Axial and sagittal orientation of the SWI images were reconstructed in-plane with a slice thickness of 0.52 mm. In addition, minimum intensity projections (MIP) of the SWI (SWI-MIP) datasets were reconstructed with a slice thickness of 4.0 mm (coronal), respectively 4.16 mm (axial/sagittal).

Qualitative evaluation of the data

Two neuroradiologists independently analyzed the delineation of the ZI to the adjacent structures for each data-

Table 1 Magnetic resonance imaging parameters for each sequence used in this study

	TR (ms)	TE (ms)	Flip angle (°)	FOV (mm)	Matrix	Resolution (mm)	Slice thickness (mm)	NoA	Receiver bandwidth (Hz/pixel)	Scan time (min)	Slice orientation
T1-GRE	6.6	2.38	12	230 × 230	448 × 448	0.513 × 0.513	0.649	1	310	06:38	Sagittal
T2-TSE tra	12 000	57	90	178 × 220	624 × 768	0.286 × 0.286	2	1	100	04:37	Axial
FLASH2D-T2Star tra	504	17	30	176 × 176	704 × 704	0.25 × 0.25	2	1	40	05:55	Axial
FLASH2D-T2Star cor	504	17	30	176 × 176	704 × 704	0.25 × 0.25	2	1	40	05:55	Coronal
FLASH2D-T2Star sag	504	17	30	176 × 176	704 × 704	0.25 × 0.25	2	1	40	06:49	Sagittal
SWI cor	13.3	21	5	149 × 199	288 × 384	0.52 × 0.52	0.5	2	120	13:21	Coronal

T1-GRE: T1-weighted gradient-echo; T2-TSE: T2-turbo spin-echo; SWI: Susceptibility-weighted imaging; TR: Time of repetition; TE: Time of echo; FOV: Field of view; NoA: Numbers of averages; tra: Transversal; cor: Coronal; sag: Sagittal.

set. The borders of the ZI were defined on the basis of anatomical and MRI data^[21,26].

Viewing and analysis of the acquired datasets were performed electronically on a DICOM workstation using OsiriX Imaging Software (<http://www.osirix-viewer.com/index.html>). Raters were allowed to freely adjust window/level settings.

The delineation of the ZI *vs* the Ci, the ZI *vs* the STN, and the ZI *vs* the PPF was assessed on the basis of each reader's own professional judgment using a 6-point scale (5 - excellent delineation; 4 - good delineation; 3 - moderate delineation; 2 - poor delineation; 1 - no delineation; 0 - no image/not evaluable).

The image quality of each sequence regarding artifacts was determined by consensus of the two readers using a 6-point grading system. The grading was as follows: 5 - no artifacts; 4 - minimal artifacts; 3 - moderate artifacts; 2 - significant artifacts; 1 - massive artifacts; 0 - no image/not evaluable.

Statistical analysis

Quantitative analyses [contrast-to-noise ratios (CNR) and signal-to-noise ratios (SNR)] for the ZI were assessed for the acquired sequences by using the Osirix-software. Each dataset was carefully scrutinized to identify the sections with the structures of interest.

The mean signal intensity (SI) was measured for all datasets, considering intra-individual identical localization, by manually placing a region of interest (ROI) of approximately 0.05 cm² within the ZI and a ROI of approximately 0.1 cm² within the Ci. The average standard deviation of noise was determined by manually placing a ROI (approximately 2.0 cm²) outside the brain and away from phase-encoding artifacts. Identical ROI sizes were used for all corresponding images. ROI measurements were repeated three times and average values were taken.

CNR and SNR for the ZI were computed for each of the nine participants (18 cerebral hemispheres) according to the equations:

$$\text{CNR} = (\text{SI}_{\text{ZI}} - \text{SI}_{\text{Ci}}) / \sigma,$$

$$\text{SNR} = \text{SI}_{\text{ZI}} / \sigma,$$

where SI_{ZI} specifies the measured mean signal within the ZI, SI_{Ci} the mean signal value in the internal capsule, and σ the average standard deviation of the noise.

To allow an easy clinical implementation we used

pulse sequences from the vendor and adapted pixel size and slice thickness. In general, SNR and CNR are linear proportional to the slice thickness and pixel size^[45]. Hence, to additionally obtain geometrically comparable SNRs and CNRs the directly measured values were adjusted to a voxel of 1 mm³ × 1 mm³ × 1 mm³. This geometrical correction of the SNR and CNR values has been used previously to quantitatively compare various sequences differing in voxel size^[46].

Statistical calculations were conducted using the Statistical Package for the Social Sciences software (SPSS 19, IBM Corporation, Somers, NY, United States). Cohen's kappa coefficient (κ) was used to assess the interrater reliability for the delineation of the ZI^[47].

Kappa values were categorized as < 0 indicating no agreement, 0-0.20 as slight, 0.21-0.40 as fair, 0.41-0.60 as moderate, 0.61-0.80 as substantial and 0.81-1 as almost perfect agreement^[48,49].

A *P* value less than 0.05 will be considered as statistically significant. Differences in delineation, SNR and CNR between the sequences were statistically evaluated using a paired *t*-test.

Co-registration of the a coronal FLASH2D-T2Star image with the corresponding coronal section schema of the Schaltenbrand and Wahren atlas

The coronal a FLASH2D-T2Star image at the level of the ZI, approximately 2 mm anterior to the midcommissural point, was co-registered with the corresponding digitized coronal section of the Schaltenbrand and Wahren atlas for stereotaxy of the human brain (plate 27)^[21]. For the overlay distinct anatomic structures in the MR image (*e.g.*, lateral wall of the third ventricle, and globus pallidus) were used. The position of the ZI was judged to be within or outside of the limits of the atlas schema.

RESULTS

Images of a representative healthy volunteer at the level of the ZI in axial (tra), coronal (cor), and sagittal (sag) orientation are displayed in Figures 1-3, respectively.

Qualitative results

All acquired images were evaluable except for the SWI

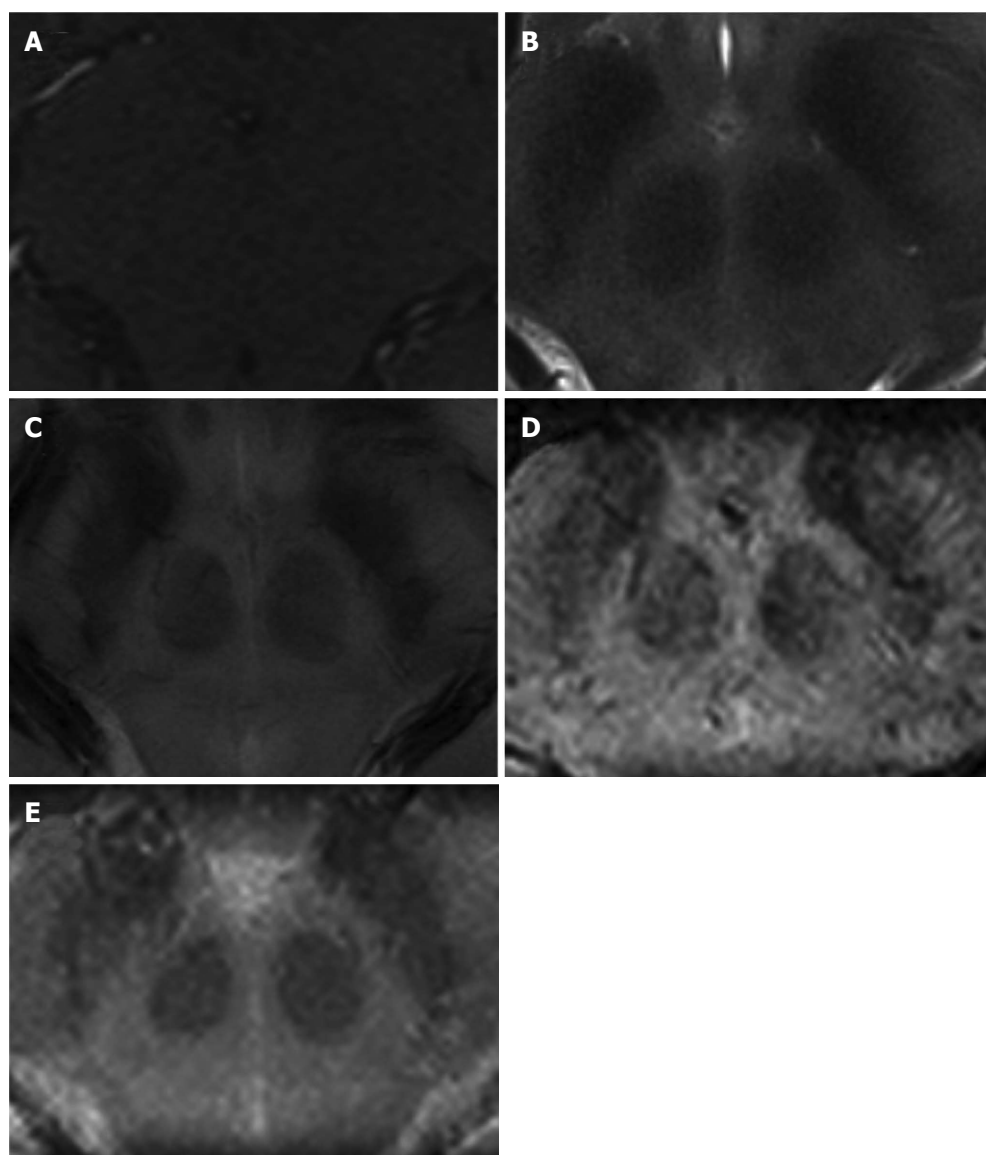


Figure 1 Representative enlarged axial view of the zona incerta. A: T1-weighted gradient-echo transversal; B: T2-turbo spin-echo transversal; C: FLASH2D-T2Star transversal; D: Susceptibility-weighted imaging (SWI) transversal; E: SWI-minimum intensity projections transversal.

sequence of one participant, which had to be excluded due to significant motion artifacts. Moderate artifacts were found for susceptibility-weighted imaging (SWI and SWI-MIP), minimal artifacts were visible in T2-TSE, and FLASH2D-T2Star imaging, and no artifacts within the ROI were seen in T1-GRE (tra, cor and sag) (Table 2).

The initial assessment of the acquired images revealed that the rZI could easily be delineated whereas the cZI was not discernable in any of the sequences. For the subsequent analysis we therefore focused on the rZI. Qualitative ratings are summarized in Figure 4.

Regarding inter-rater reliability, identical results of both readers were seen for the delineation of the rZI *vs* the Ci, the rZI *vs* the STN, and the rZI *vs* the PFF in T1-GRE imaging (tra, cor and sag) ($\kappa = 1$). For T2-TSE varying results were obvious with perfect agreement for the delineation of the rZI *vs* the STN and *vs* the PFF, and slight agreement for the distinction of the rZI *vs* the

Ci. Fair agreement was found for FLASH2D-T2Star sag imaging for the delineation of the rZI *vs* the Ci and for SWI-MIP cor imaging for the distinction of the rZI *vs* the PFF. The inter-rater reliability for FLASH2D-T2Star, SWI, and SWI-MIP (all orientations) was at least moderate.

In terms of delineation the T1-weighted images provided, besides a good contrast between cortex and white matter, only little contrast between the midbrain structures resulting in no obvious delineation of the Ci, the STN, and the PFF *vs* the ZI in all views. The T2-TSE images demonstrated good contrast for the grey matter. However, the rZI *vs* the Ci could only be delineated poorly. In addition delineation between the ZI and the STN, respectively between the ZI and the PFF was impossible. In contrast, SWI (SWI and SWI-MIP) and FLASH2D-T2Star images provided a considerably better demarcation of the rZI. Especially the coronal ori-

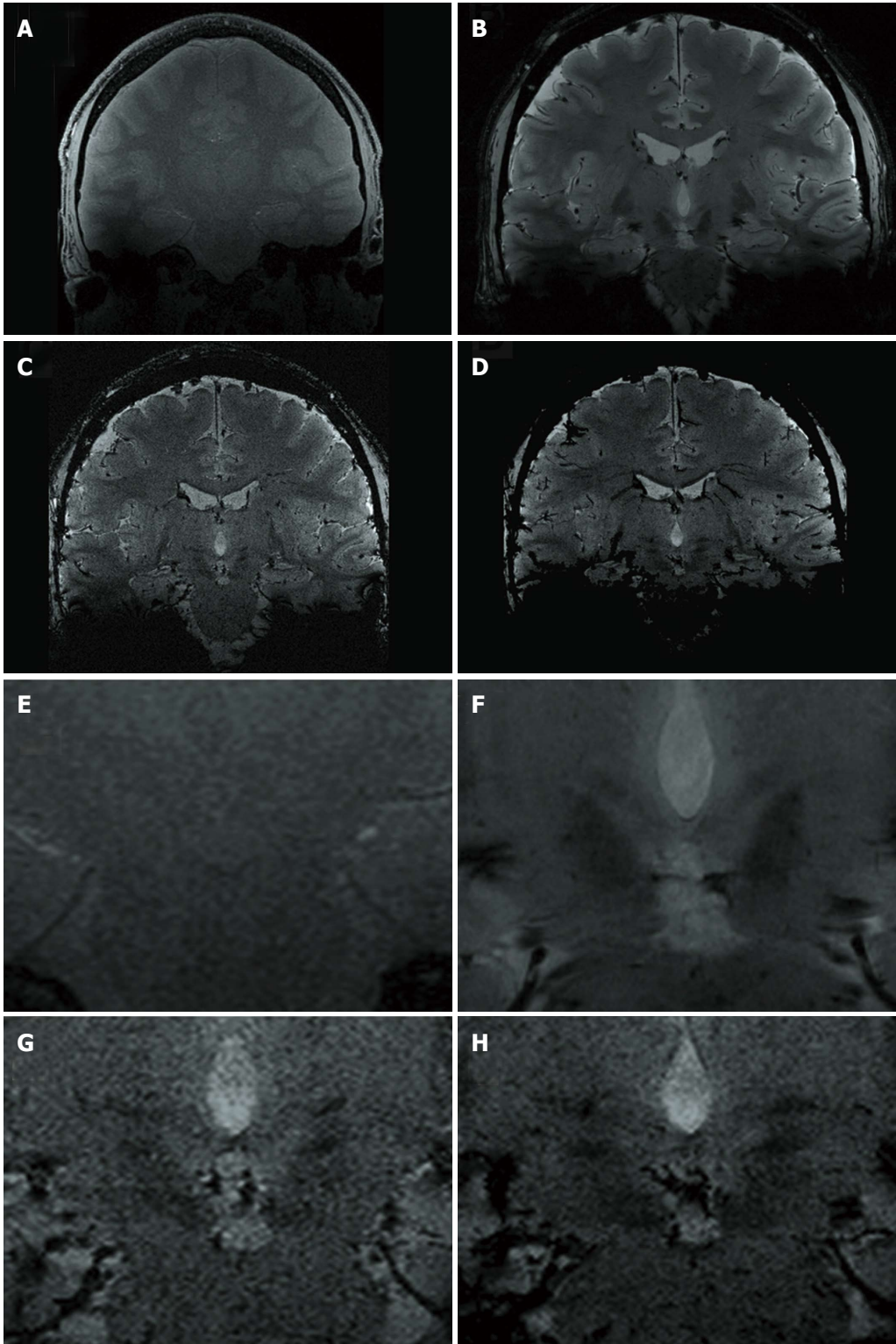


Figure 2 Non-enlarged (A-D) and enlarged (E-H) representative coronal images at the level of the zona incerta. A, E: T1-weighted gradient-echo coronal; B, F: FLASH2D-T2Star coronal; C, G: Susceptibility-weighted imaging (SWI) coronal; D, H: SWI-minimum intensity projections coronal.

entation and to a lesser degree the sagittal orientation showed a clear boundary dividing the rZI from the Ci, the STN, and the PFF. Moreover, the rZI was discernible in coronal FLASH2D-T2Star images in all nine healthy volunteers in both hemispheres (Figure 5).

In comparison to the current standard sequence used

for DBS targeting (T2-TSE) particularly the coronal and to a lesser degree the sagittal the FLASH2D-T2Star, as well as the SWI sequences (SWI and SWI-MIP) provided also statistically a significant superior delineation ($P < 0.001$) of the rZI *vs* the Ci, *vs* the STN, and *vs* the PFF (Figure 4).

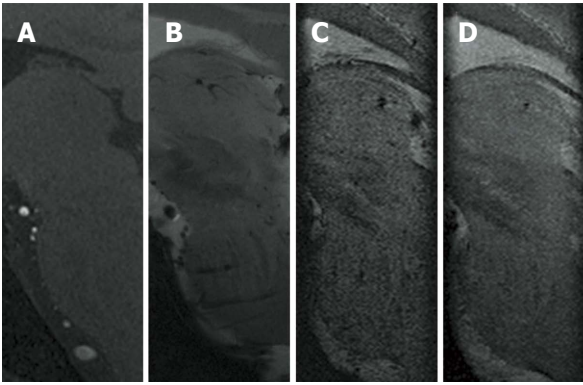


Figure 3 Representative enlarged visualization of the zona incerta in sagittal view. A: T1-weighted gradient-echo sagittal; B: FLASH2D-T2Star sagittal; C: Susceptibility-weighted imaging (SWI) sagittal; D: SWI-minimum intensity projections sagittal.

Table 2 Image quality in terms of artifacts at the level of the zona incerta

Sequence	Consensus of two readers
T1-GRE tra	5.00 ± 0.00
T1-GRE-cor	5.00 ± 0.00
T1-GRE sag	5.00 ± 0.00
T2-TSE tra	4.78 ± 0.43
FLASH2D-T2Star tra	3.94 ± 0.54
FLASH2D-T2Star cor	3.94 ± 0.73
FLASH2D-T2Star sag	3.94 ± 0.64
SWI tra	2.92 ± 0.62
SWI cor	2.79 ± 0.43
SWI sag	3.00 ± 0.39
SWI-MIP tra	2.57 ± 0.51
SWI-MIP cor	2.64 ± 0.50
SWI-MIP sag	2.57 ± 0.51

Image quality in terms of artifacts at the level of the zona incerta was evaluated for each sequence by consensus of two radiologists using a 6-scale grading system (5: no artifacts; 4: minimal artifacts; 3: moderate artifacts; 2: significant artifacts; 1: massive artifacts; 0: no image/not evaluable). T1-GRE: T1-weighted gradient-echo; T2-TSE: T2-turbo spin-echo; SWI: Susceptibility-weighted imaging; MIP: Minimum intensity projections transversal; tra: Transversal; cor: Coronal; sag: Sagittal.

Quantitative results

To provide directly clinical relevant information, we analyzed the SNR and CNR of the sequences as acquired (non-adjusted for voxel-size). Additionally we adjusted the measurements for a comparison independent of the acquired voxel size. SNR and CRN measurements for the rZI are shown in Table 3.

The non-adjusted SNRs of the rZI in SWI-MIP, T1-GRE, and FLASH2D-T2Star images were significantly higher compared to T2-TSE. Non-MIP SWI images provided slightly higher SNRs compared to T2-TSE, yet without a statistical significance. The adjusted SNR differ only slightly: Similarly, SWI-MIP, T1-GRE, and FLASH2D-T2Star images showed significantly higher SNR values compared to T2-TSE. Besides, also coronal SWI images showed a slight, significantly higher SNR compared to T2-TSE images.

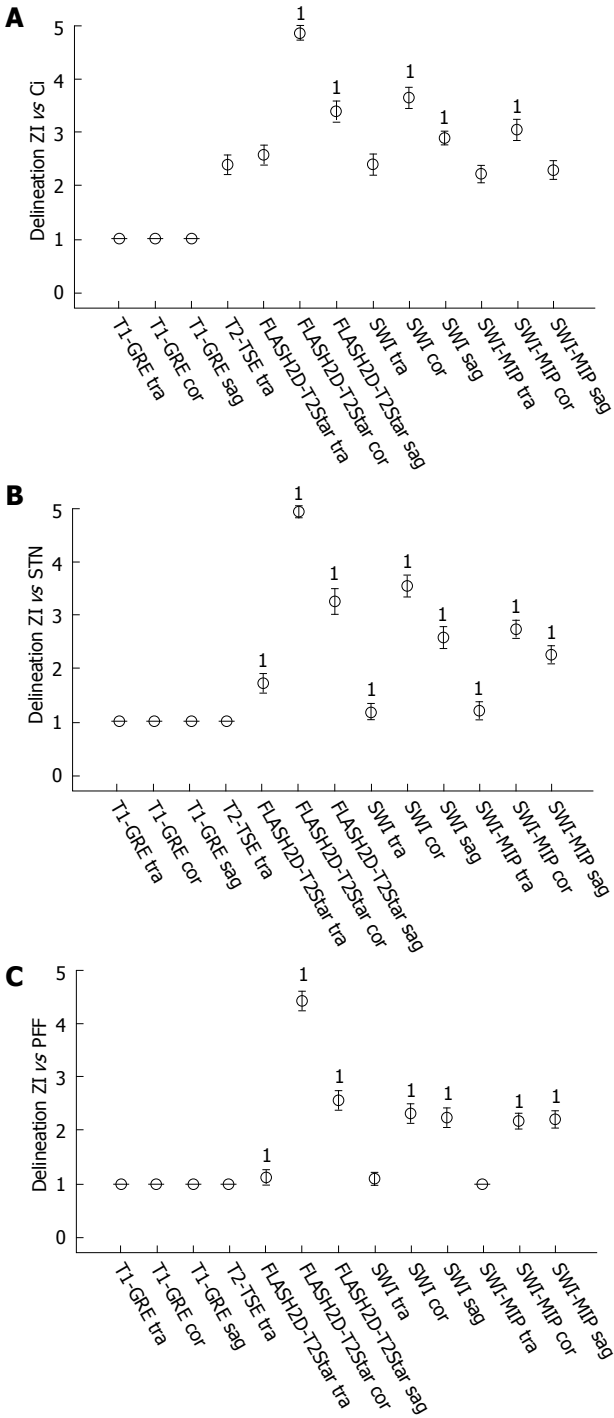


Figure 4 Qualitative ratings. A: Average delineation of the zona incerta (ZI) vs the internal capsule; B: ZI vs the subthalamic nucleus; C: ZI vs pallidofugal fibres. The table (left) indicates the average delineation and the standard deviation of the mean as well as the inter-rater reliability (κ) with its statistically significance (P value). The diagram (right) demonstrates the average delineation for the ZI, error bars indicate the 95%CI of the mean. Sequences with a statistically significant superior delineation compared to T2-TSE imaging (paired t -test) are denoted (1).

After calculation of the SNR and according to the Rose criterion^[50] all scans allowed the recognition of image features with a 100% certainty (all SNR values are higher than 5).

SWI-MIP showed the best non-adjusted CNR with

Table 3 Average signal-to-noise ratios and contrast-to-noise-ratios of the zona incerta at 7.0 T magnetic resonance imaging

Sequence	SNR		CNR	
	Non-adjusted	Adjusted	Non-adjusted	Adjusted
T1-GRE tra	46.30 ± 9.48 ¹	271.09 ± 55.51 ¹	6.14 ± 2.01	35.96 ± 11.79
T1-GRE cor	46.33 ± 8.88 ¹	271.23 ± 55.98 ¹	6.47 ± 2.12	37.87 ± 12.42
T1-GRE sag	45.75 ± 9.44 ¹	267.84 ± 55.24 ¹	7.05 ± 2.67	41.30 ± 15.63
T2-TSE tra	17.18 ± 6.51	105.03 ± 39.81	19.40 ± 4.20	121.69 ± 25.68
FLASH2D-T2Star tra	40.28 ± 16.32 ¹	322.23 ± 130.60 ¹	44.17 ± 12.90 ¹	353.33 ± 103.19 ¹
FLASH2D-T2Star cor	53.06 ± 11.09 ¹	424.48 ± 88.76 ¹	31.76 ± 8.281	254.08 ± 66.24 ¹
FLASH2D-T2Star sag	57.84 ± 10.31 ¹	462.75 ± 88.76 ¹	33.92 ± 11.76 ¹	271.39 ± 94.05 ¹
SWI tra	18.94 ± 6.98	140.05 ± 51.62	10.99 ± 4.94	81.26 ± 36.57
SWI cor	19.20 ± 8.23	141.98 ± 60.88	10.40 ± 4.35	76.95 ± 32.15
SWI sag	18.80 ± 7.52	139.05 ± 55.65	11.07 ± 4.30	81.90 ± 31.85
SWI-MIP tra	358.89 ± 152.81 ¹	331.81 ± 141.28 ¹	275.70 ± 127.52 ¹	254.90 ± 117.90 ¹
SWI-MIP cor	354.00 ± 116.37 ¹	327.29 ± 107.59 ¹	275.86 ± 121.59 ¹	255.05 ± 112.41 ¹
SWI-MIP sag	312.66 ± 8.44 ¹	289.07 ± 75.29 ¹	261.28 ± 121.88 ¹	241.57 ± 119.15 ¹

¹To further compare differences of the directly computed signal-to-noise ratios (SNR) and contrast-to-noise-ratios (CNR) values (non-adjusted), the obtained results for each sequence were adjusted to a voxel of 1 mm³ × 1 mm³ × 1 mm³, by applying an associated conversion factor. Sequences with statistically significant superior SNR and CNR values compared to T2-TSE imaging (paired *t*-test) are denoted. T1-GRE: T1-weighted gradient-echo; T2-TSE: T2-turbo spin-echo; SWI: Susceptibility-weighted imaging; MIP: Minimum intensity projections transversal; tra: Transversal; cor: Coronal; sag: Sagittal.

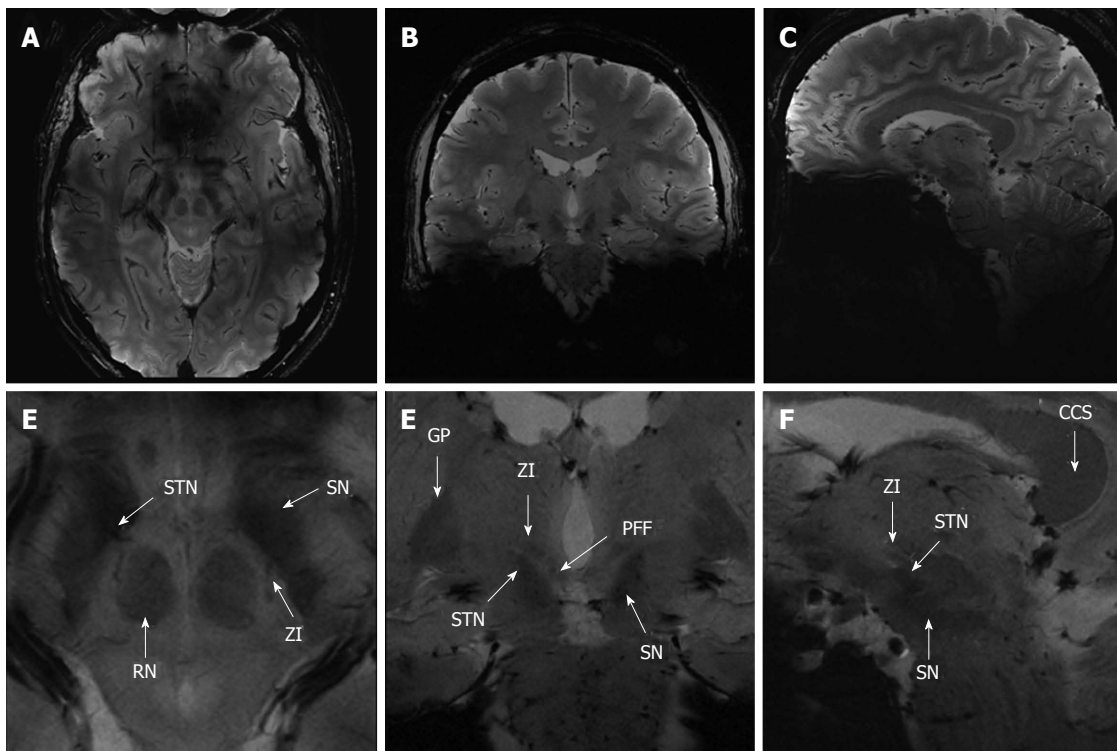


Figure 5 Illustration of the subthalamic area in FLASH2D-T2Star (A, B, C; magnified in D, E, F). The zona incerta (ZI) and the surrounding structures are indicated. STN: Subthalamic nucleus; PFF: Pallidofugal fibres; SN: Substantia nigra; RN: Red nucleus; GP: Globus pallidus; CCS: Splenium corporis callosi.

significant higher measurements relative to the T2-TSE images for the rZI. FLASH2D-T2Star imaging provided a lower, still significantly higher CNR compared to T2-TSE imaging. SWI and T1-GRE images, in contrast, showed the least non-adjusted CNRs of all acquired sequences, below the CNR values for T2-TSE imaging. After adjustment of the directly measured CNR values to a voxel volume of 1 mm³ similar result were obtained: SWI-MIP and FLASH2D-T2Star imaging provided sig-

nificantly higher CNR values compared to T2-TSE images for the rZI. The lowest CNRs were calculated for T1-GRE imaging.

Intraindividual comparison of 3.0 T and 7.0 T

Figure 6 illustratively opposes 3.0 T and 7.0 T images of one volunteer (coronal FLASH2D-T2Star). 7.0 T provides a much sharper delineation of the rZI with substantially higher contrast.

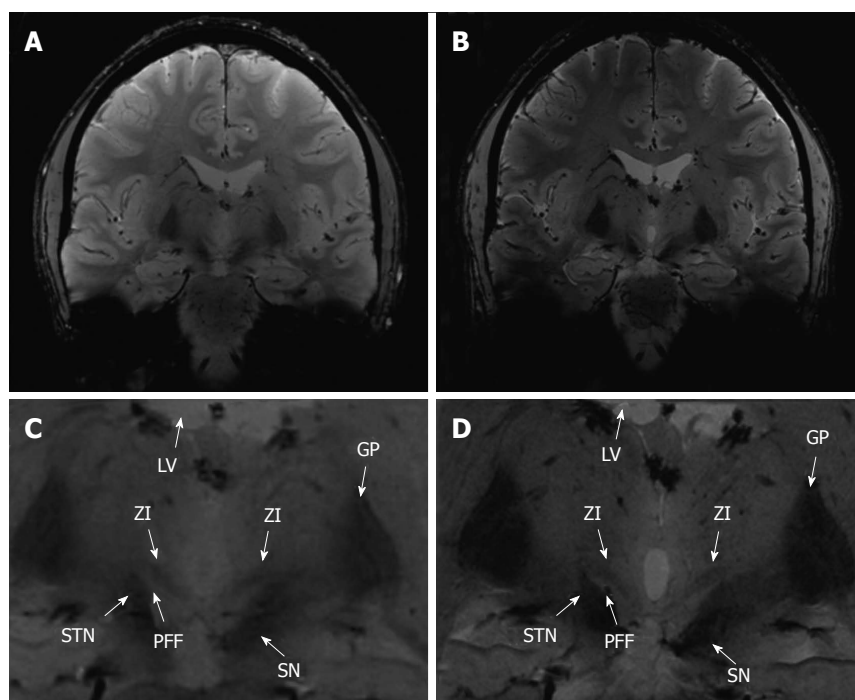


Figure 6 Illustration of the subthalamic area in coronal FLASH2D-T2Star imaging at 3.0 Tesla (A; magnified in C) and 7.0 Tesla (B; magnified in D). The zona incerta (ZI) and the surrounding structures are indicated. STN: Subthalamic nucleus; PFF: Pallidofugal fibres; SN: Substantia nigra; GP: Globus pallidus; LV: Lateral ventricle.

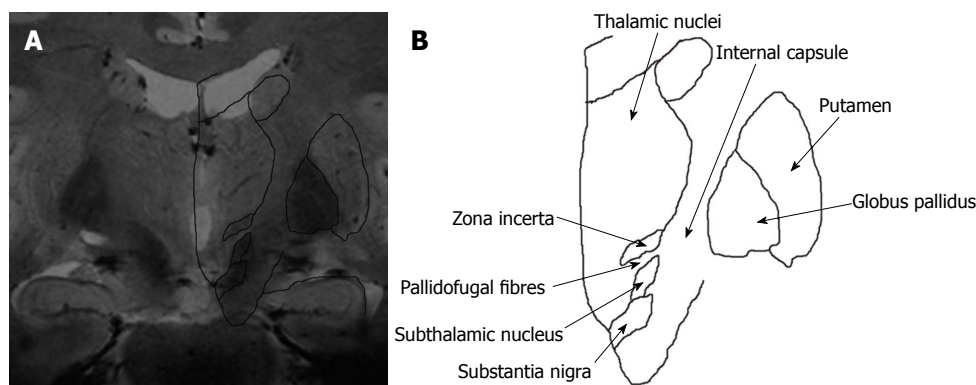


Figure 7 Co-registration of a coronal FLASH2D-T2Star image at the level of the zona incerta with a coronal schematic drawing of the deep brain nuclei (due to license issues the respective image from the Schaltenbrand and Wahren atlas is currently not available for open-access publication) (A), schematic drawing, at the level of the zona incerta (B). The zona incerta is demarcated as a hypointense structure cranial to the subthalamic nucleus.

Co-registration of the coronal section of the Schaltenbrand and Wahren atlas with the coronal FLASH2D-T2Star imaging

To verify the anatomical correctness we co-registered the coronal FLASH2D-T2Star image at the level of the rZI (approximately 2 mm anterior to the midcommissural point) with the widely used atlas for brain surgery, the Schaltenbrand and Wahren atlas for stereotaxy of the human brain^[21]. With the help of the schema an easy identification of the ZI was possible. The ZI projected into the boundaries of the anatomical schema in all 18 cases. Figure 7 illustrates a co-registration of the respective coronal FLASH2D-T2Star image with a coronal schematic drawing of the deep brain nuclei (due to license issues the respective image from the Schaltenbrand

and Wahren atlas is currently not available for open-access publication).

DISCUSSION

DBS is a reversible stereotactic long-term therapeutic option for patients with chronic movement disorders including PD and tremor^[1,51]. The method plays, after the approval by the US Food and Drug Administration, an accepted role in the treatment of medically refractory movement disorders including ET^[52].

Progress in medical imaging has improved the visualization of the DBS target structures. In the era of 1.5 T the direct visualization failed, secondary to insufficient contrast and low resolution^[27,53]. At 3.0 T initial promis-

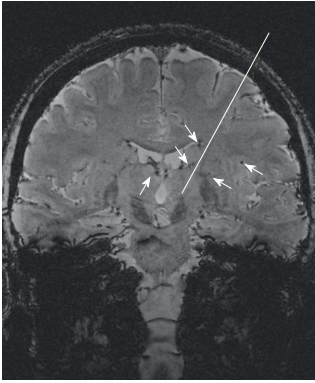


Figure 8 The use of susceptibility-weighted imaging for stereotactic navigation. In the coronal susceptibility-weighted imaging at the level of the zona incerta the deep cerebral veins and tiny transparenchymal vessels (arrows) can be easily identified. Thereby the trajectory (white line) can be readjusted to avoid hemorrhage.

ing results for the visualization of the ZI have been presented^[54]. The implementation of 7.0 T MRI is a further technical advance to a higher signal and a superior spatial resolution compared to 1.5 T and 3.0 T^[27,37,55]. Nevertheless, due to its localization in the subthalamic region, adjacent to a number of vital structures^[19,20,28], the ZI is difficult to visualize and localize. Hence, the use of 7.0 T MRI may facilitate the direct visualization of the ZI.

This is the first study to present data on the visualization of the ZI at 7.0 T. A key finding of our analysis is that the rZI can be visualized easily. The cZI cannot be discerned using the sequences of this study. This finding has to be kept in mind for the pre-stereotactic planning of the ZI on the basis of MRI. Consequently, the rZI can be used as a landmark for targeting of the adjacent cZI. We hypothesize that the diverging visualization of rZI and cZI is secondary to its heterogeneous histological composition (that also become obvious in the diverse appearance on the histological sections of the stereotactic atlas^[21]).

In our qualitative as well as our quantitative analysis the rZI was optimally delineated in the FLASH2D-T2Star sequence, especially in coronal orientation.

For the implementation of image-guided stereotactic neurosurgery a sufficiently high inter-rater reliability of the radiological evaluation is crucial. To our knowledge, inter-rater reliability has not yet been assessed for the visualization of the ZI at 7.0 T. In our analysis, the inter-rater reliability of the most adequate sequence for the visualization of the rZI, the coronal FLASH2D-T2Star, was substantial for the demarcation of the rZI versus the Ci, the STN and the PFF.

In summary, these results indicate that the most adequate sequence at 7.0 T MRI for the imaging of the ZI, the coronal FLASH2D-T2Star, allows a reliable pre-stereotactic visualization of the rZI if performed by readers experienced in the imaging of deep brain nuclei. Nevertheless, further optimization of the sequences is required to ameliorate the inter-rater reliability.

In our study the rZI was optimally delineated in se-

quences susceptible to local field inhomogeneities. Although the chemical composition of the ZI is yet not exactly known, we assume that the signal characteristics of the rZI are caused by iron deposits^[20].

The association between iron deposition and neurodegenerative diseases has been described before^[56,57]. Particularly in deep brain structures of PD patients (subthalamic region and basal ganglia) a progressive increase of iron concentration has been reported^[58]. While iron accumulation seems to be a result of non-specific neuronal degeneration, the exact relation between iron deposition and neurodegenerative diseases remains still unknown^[20].

Gelman *et al*^[59] initially reported that the SI of the basal ganglia on T2-weighted images primarily depends on the iron concentration. Similarly, in T2*- and susceptibility weighted images the high iron concentration results in a hypointense signal of the STN and internal globus pallidus^[20,31]. We found a hypointense signal in the rZI in sequences that are susceptible to local field inhomogeneities and therefore assume that the signal characteristics of the rZI are analogously caused by iron deposition. This iron deposition in the rZI may render patients affected by neurodegenerative diseases especially suitable for T2*, T2*-FLASH2D and SWI imaging. It is therefore necessary to further validate our findings (young and healthy population) in a patient cohort.

As an additional benefit, SWI, originally developed to track blood oxygen saturation^[44], provides a clear visualization of deep cerebral veins and transparenchymal vessels. These anatomic details may help the neurosurgeon in the pre-operative planning to avoid predictable intracranial hemorrhages due to blood vessel injuries (Figure 8)^[60].

Initially, geometrical distortions and susceptibility artifacts have been assumed to complicate an accurate DBS navigation with MRI (especially at 7 T). However, different studies demonstrate that the targeting error for structures located within the center of the brain away from air-filled cavities (like the ZI) is in the submillimeter range. Initial reports at 1.5 T found distortions of T2-TSE to be less than one millimeter^[36]. At 3 T MRI Balachandran *et al*^[61] described the targeting error of T2-TSE in comparison to CT with a maximum of 0.13 mm over twelve targets. Duchin *et al*^[62] compared T2-TSE at 7 T and 1.5 T and found distortion differences of less than one voxel size. At 7 T MRI Cho *et al*^[27] quantified the geometrical distortions of a T2-weighted gradient-echo sequence with a mean deviation of 0.12 ± 0.13 mm.

Our results confirm these findings. In the co-registration the rZI projected in its boundaries of the anatomic schema^[21] in all 18 cases. This supports the correct identification of the rZI and affirms the anatomic accuracy of the technique.

Furthermore, current evolutions in MR methodology, including B₀ shimming^[63] as well as the use of commercially pre-installed second-order active shimming^[27] may further compensate geometrical distortions caused by the high magnetic field.

In conclusion, the rZI is precisely and reliably visualized by FLASH2D-T2Star imaging at 7.0 T (particularly

in the coronal view), whereas the cZI is not identifiable in any of the sequences tested. These results facilitate enhanced and more precise targeting of the cZI. Therefore intervention time and complication rates in DBS surgery may be reduced substantially in the future.

COMMENTS

Background

Deep brain stimulation (DBS) is an accepted neurosurgical technique for the treatment of many neurological and psychiatric disorders, such as Parkinson's disease, essential tremor, dystonia. The subthalamic nucleus (STN) represents the commonly chosen target site to suppress resting tremor in patients with Parkinson's disease. However, several clinical trials have reported negative limbic effects of STN DBS, including depression, apathy and decreased cognitive function. Therefore, the zona incerta (ZI) has been proposed as an alternative target area. For the exact stereotactical planning optimal delineation of the ZI by magnetic resonance imaging (MRI) has to be achieved.

Research frontiers

Up to now, MRI data concerning the ZI is sparse. One study at 3.0 Tesla (T) reports that the visualization of the ZI is feasible but limited due to lack of signal and spatial resolution. With the higher field strength 7.0 T has the potential to improve the discernibility of the ZI.

Innovations and breakthroughs

For the first time, different sequences and orientations were evaluated to find the currently optimal combination for the visualization of the ZI at 7.0 T. Intra-individual comparison between 3.0 and 7.0 T demonstrated a clearly superior delineation and substantially higher contrast using the higher field strength. The rostral part of the ZI (rZI) could easily be identified and was best and reliably visualized in the coronal FLASH2D-T2Star images. The caudal part (cZI) was not definable in any of the sequences. FLASH2D-T2Star and susceptibility-weighted imaging offered significant higher contrast-to-noise ratios for the rZI compared T2-turbo spin-echo (T2-TSE). T1-gradient-echo and T2-TSE were clearly inferior both in quantitative and qualitative analysis. The co-registration of the coronal FLASH2D-T2Star images with the stereotactical atlas schema (Schaltenbrand-Wahren) confirmed the correct localization of the ZI in all cases.

Applications

The results provide the currently optimal delineation of the rZI at 7.0 T. These results can facilitate a better and more precise targeting of the cZI.

Terminology

DBS is a treatment option in several medication refractory neurological disorders. The method consists in inserting a small electrode through the brain parenchyma to a small specific target region in the area of the deep brain nuclei.

Peer review

The manuscript submitted by the authors for publication demonstrates the merits of 7.0T MRI of the ZI for the purpose of DBS treatment planning. The subject matter is interesting and current and the authors provide a thorough bibliographical introduction in order to set the context for the objective of their research. The materials and methods are sufficiently described and the results are presented in a concise and informative way. The discussion of the results outlines both the author's conclusions and avenues of further research. It is still the recommendation for priority publication of this article.

REFERENCES

- 1 **Deep-Brain Stimulation for Parkinson's Disease Study Group.** Deep-brain stimulation of the subthalamic nucleus or the pars interna of the globus pallidus in Parkinson's disease. *N Engl J Med* 2001; **345**: 956-963 [PMID: 11575287 DOI: 10.1056/NEJMoa000827]
- 2 **Kim HJ, Jeon BS, Paek SH, Lee JY, Kim HJ, Kim CK, Kim DG.** Bilateral subthalamic deep brain stimulation in Parkinson disease patients with severe tremor. *Neurosurgery* 2010; **67**: 626-632; discussion 632 [PMID: 20647970 DOI: 10.1227/01.NEU.0000374850.98949.D4]
- 3 **Rehncrona S, Johnels B, Widner H, Törnqvist AL, Hariz M, Sydow O.** Long-term efficacy of thalamic deep brain stimulation for tremor: double-blind assessments. *Mov Disord* 2003; **18**: 163-170 [PMID: 12539209 DOI: 10.1002/mds.10309]
- 4 **Tisch S, Rothwell JC, Limousin P, Hariz MI, Corcos DM.** The physiological effects of pallidal deep brain stimulation in dystonia. *IEEE Trans Neural Syst Rehabil Eng* 2007; **15**: 166-172 [PMID: 17601185 DOI: 10.1109/TNSRE.2007.896994]
- 5 **Castrioto A, Lozano AM, Poon YY, Lang AE, Fallis M, Moro E.** Ten-year outcome of subthalamic stimulation in Parkinson disease: a blinded evaluation. *Arch Neurol* 2011; **68**: 1550-1556 [PMID: 21825213]
- 6 **Mandat T, Tykocki T, Koziara H, Kozirowski D, Brodacki B, Rola R, Bonicki W, Nauman P.** Subthalamic deep brain stimulation for the treatment of Parkinson disease. *Neurol Neurochir Pol* 2011; **45**: 32-36 [PMID: 21384291]
- 7 **Bejjani BP, Damier P, Arnulf I, Thivard L, Bonnet AM, Dormont D, Cornu P, Pidoux B, Samson Y, Agid Y.** Transient acute depression induced by high-frequency deep-brain stimulation. *N Engl J Med* 1999; **340**: 1476-1480 [PMID: 10320386 DOI: 10.1056/NEJM199905133401905]
- 8 **Umemura A, Oka Y, Yamamoto K, Okita K, Matsukawa N, Yamada K.** Complications of subthalamic nucleus stimulation in Parkinson's disease. *Neurol Med Chir (Tokyo)* 2011; **51**: 749-755 [PMID: 22123476]
- 9 **Hamel W, Fietzek U, Morsnowski A, Schrader B, Herzog J, Weinert D, Pfister G, Müller D, Volkmann J, Deuschl G, Mehdorn HM.** Deep brain stimulation of the subthalamic nucleus in Parkinson's disease: evaluation of active electrode contacts. *J Neurol Neurosurg Psychiatry* 2003; **74**: 1036-1046 [PMID: 12876231]
- 10 **Herzog J, Fietzek U, Hamel W, Morsnowski A, Steigerwald F, Schrader B, Weinert D, Pfister G, Müller D, Mehdorn HM, Deuschl G, Volkmann J.** Most effective stimulation site in subthalamic deep brain stimulation for Parkinson's disease. *Mov Disord* 2004; **19**: 1050-1054 [PMID: 15372594 DOI: 10.1002/mds.20056]
- 11 **Voges J, Volkmann J, Allert N, Lehrke R, Koulousakis A, Freund HJ, Sturm V.** Bilateral high-frequency stimulation in the subthalamic nucleus for the treatment of Parkinson disease: correlation of therapeutic effect with anatomical electrode position. *J Neurosurg* 2002; **96**: 269-279 [PMID: 11838801 DOI: 10.3171/jns.2002.96.2.0269]
- 12 **Blomstedt P, Sandvik U, Linder J, Fredricks A, Forsgren L, Hariz MI.** Deep brain stimulation of the subthalamic nucleus versus the zona incerta in the treatment of essential tremor. *Acta Neurochir (Wien)* 2011; **153**: 2329-2335 [PMID: 21904970 DOI: 10.1007/s00701-011-1157-4]
- 13 **Sandvik U, Hariz GM, Blomstedt P.** Quality of life following DBS in the caudal zona incerta in patients with essential tremor. *Acta Neurochir (Wien)* 2012; **154**: 495-499 [PMID: 22109693 DOI: 10.1007/s00701-011-1230-z]
- 14 **Mitrofanis J.** Some certainty for the "zone of uncertainty"? Exploring the function of the zona incerta. *Neuroscience* 2005; **130**: 1-15 [PMID: 15561420]
- 15 **Jones EG.** The Thalamus. New York: Plenum Press, 1985
- 16 **Mitrofanis J, Ashkan K, Wallace BA, Benabid AL.** Chemoarchitectonic heterogeneities in the primate zona incerta: clinical and functional implications. *J Neurocytol* 2004; **33**: 429-440 [PMID: 15520528]
- 17 **Mok D, Mogenson GJ.** Convergence of signals in the zona incerta for angiotensin-mediated and osmotic thirst. *Brain Res* 1987; **407**: 332-340 [PMID: 3567649]
- 18 **Plaha P, Khan S, Gill SS.** Bilateral stimulation of the caudal zona incerta nucleus for tremor control. *J Neurol Neurosurg Psychiatry* 2008; **79**: 504-513 [PMID: 18037630]
- 19 **Carpenter M.** The subthalamic region. In: Carpenter Me, editor. Human Neuroanatomy. Baltimore: Williams and Wilkins, 1976: 509-511
- 20 **Dormont D, Ricciardi KG, Tandé D, Parain K, Menuel C, Galanaud D, Navarro S, Cornu P, Agid Y, Yelnik J.** Is the

- subthalamic nucleus hypointense on T2-weighted images? A correlation study using MR imaging and stereotactic atlas data. *AJNR Am J Neuroradiol* 2004; **25**: 1516-1523 [PMID: 15502130]
- 21 **Schaltenbrand G**, Wahren W. Atlas for Stereotaxy of the Human Brain. 2nd ed. Stuttgart: Thieme, 1977
 - 22 **Yelnik J**, Percheron G. Subthalamic neurons in primates: a quantitative and comparative analysis. *Neuroscience* 1979; **4**: 1717-1743 [PMID: 117397]
 - 23 **Burrows AM**, Ravin PD, Novak P, Peters ML, Dessureau B, Swearer J, Pilitsis JG. Limbic and motor function comparison of deep brain stimulation of the zona incerta and subthalamic nucleus. *Neurosurgery* 2012; **70**: 125-130; discussion 130-131 [PMID: 21869721 DOI: 10.1227/NEU.0b013e318232fdac]
 - 24 **Plaha P**, Filipovic S, Gill SS. Induction of parkinsonian resting tremor by stimulation of the caudal zona incerta nucleus: a clinical study. *J Neurol Neurosurg Psychiatry* 2008; **79**: 514-521 [PMID: 18037629]
 - 25 **Plaha P**, Javed S, Agombar D, O' Farrell G, Khan S, Whone A, Gill S. Bilateral caudal zona incerta nucleus stimulation for essential tremor: outcome and quality of life. *J Neurol Neurosurg Psychiatry* 2011; **82**: 899-904 [PMID: 21285454 DOI: 10.1136/jnnp.2010.222992]
 - 26 **Plaha P**, Ben-Shlomo Y, Patel NK, Gill SS. Stimulation of the caudal zona incerta is superior to stimulation of the subthalamic nucleus in improving contralateral parkinsonism. *Brain* 2006; **129**: 1732-1747 [PMID: 16720681]
 - 27 **Cho ZH**, Min HK, Oh SH, Han JY, Park CW, Chi JG, Kim YB, Paek SH, Lozano AM, Lee KH. Direct visualization of deep brain stimulation targets in Parkinson disease with the use of 7-tesla magnetic resonance imaging. *J Neurosurg* 2010; **113**: 639-647 [PMID: 20380532 DOI: 10.3171/2010.3.JNS091385]
 - 28 **Hattingen E**, Blasel S, Nichtweiss M, Zanella FE, Weidauer S. MR imaging of midbrain pathologies. *Clin Neuroradiol* 2010; **20**: 81-97 [PMID: 20532857 DOI: 10.1007/s00062-010-0009-6]
 - 29 **Spiegelmann R**, Friedman WA. Rapid determination of thalamic CT-stereotactic coordinates: a method. *Acta Neurochir (Wien)* 1991; **110**: 77-81 [PMID: 1882723]
 - 30 **Aziz TZ**, Nandi D, Parkin S, Liu X, Giladi N, Bain P, Gregory RG, Joint C, Scott RB, Stein JF. Targeting the subthalamic nucleus. *Stereotact Funct Neurosurg* 2001; **77**: 87-90 [PMID: 12378062]
 - 31 **Brunenberg EJ**, Platel B, Hofman PA, Ter Haar Romeny BM, Visser-Vandewalle V. Magnetic resonance imaging techniques for visualization of the subthalamic nucleus. *J Neurosurg* 2011; **115**: 971-984 [PMID: 21800960 DOI: 10.3171/2011.6.JNS101571]
 - 32 **Andrade-Souza YM**, Schwalb JM, Hamani C, Eltahawy H, Hoque T, Saint-Cyr J, Lozano AM. Comparison of three methods of targeting the subthalamic nucleus for chronic stimulation in Parkinson's disease. *Neurosurgery* 2005; **56**: 360-368; discussion 360-368 [PMID: 15794832]
 - 33 **Bour LJ**, Contarino MF, Foncke EM, de Bie RM, van den Munckhof P, Speelman JD, Schuurman PR. Long-term experience with intraoperative microrecording during DBS neurosurgery in STN and GPi. *Acta Neurochir (Wien)* 2010; **152**: 2069-2077 [PMID: 20949292 DOI: 10.1007/s00701-010-0835-y]
 - 34 **Chang WS**, Kim HY, Kim JP, Park YS, Chung SS, Chang JW. Bilateral subthalamic deep brain stimulation using single track microelectrode recording. *Acta Neurochir (Wien)* 2011; **153**: 1087-1095 [PMID: 21311918 DOI: 10.1007/s00701-011-0953-1]
 - 35 **Ashkan K**, Blomstedt P, Zrinzo L, Tisch S, Yousry T, Limousin-Dowsey P, Hariz MI. Variability of the subthalamic nucleus: the case for direct MRI guided targeting. *Br J Neurosurg* 2007; **21**: 197-200 [PMID: 17453788]
 - 36 **Daniluk S**, G Davies K, Elias SA, Novak P, Nazzaro JM. Assessment of the variability in the anatomical position and size of the subthalamic nucleus among patients with advanced Parkinson's disease using magnetic resonance imaging. *Acta Neurochir (Wien)* 2010; **152**: 201-10; discussion 210 [PMID: 19806309 DOI: 10.1007/s00701-009-0514-z]
 - 37 **Abosch A**, Yacoub E, Ugurbil K, Harel N. An assessment of current brain targets for deep brain stimulation surgery with susceptibility-weighted imaging at 7 tesla. *Neurosurgery* 2010; **67**: 1745-1756; discussion 1756 [PMID: 21107206 DOI: 10.1227/NEU.0b013e3181f74105]
 - 38 **Kitajima M**, Korogi Y, Kakeda S, Moriya J, Ohnari N, Sato T, Hayashida Y, Hirai T, Okuda T, Yamashita Y. Human subthalamic nucleus: evaluation with high-resolution MR imaging at 3.0 T. *Neuroradiology* 2008; **50**: 675-681 [PMID: 18443775 DOI: 10.1007/s00234-008-0388-4]
 - 39 **Guo T**, Finnis KW, Deoni SC, Parrent AG, Peters TM. Comparison of different targeting methods for subthalamic nucleus deep brain stimulation. *Med Image Comput Comput Assist Interv* 2006; **9**: 768-775 [PMID: 17354960]
 - 40 **Gringel T**, Schulz-Schaeffer W, Elolf E, Frölich A, Dechent P, Helms G. Optimized high-resolution mapping of magnetization transfer (MT) at 3 Tesla for direct visualization of substructures of the human thalamus in clinically feasible measurement time. *J Magn Reson Imaging* 2009; **29**: 1285-1292 [PMID: 19472385 DOI: 10.1002/jmri.21756]
 - 41 **Duyn JH**, van Gelderen P, Li TQ, de Zwart JA, Koretsky AP, Fukunaga M. High-field MRI of brain cortical substructure based on signal phase. *Proc Natl Acad Sci USA* 2007; **104**: 11796-11801 [PMID: 17586684]
 - 42 **O'Gorman RL**, Shmueli K, Ashkan K, Samuel M, Lythgoe DJ, Shahidiani A, Wastling SJ, Footman M, Selway RP, Jarosz J. Optimal MRI methods for direct stereotactic targeting of the subthalamic nucleus and globus pallidus. *Eur Radiol* 2011; **21**: 130-136 [PMID: 20652256 DOI: 10.1007/s00330-010-1885-5]
 - 43 **Nölte IS**, Gerigk L, Al-Zghloul M, Groden C, Kerl HU. Visualization of the internal globus pallidus: sequence and orientation for deep brain stimulation using a standard installation protocol at 3.0 Tesla. *Acta Neurochir (Wien)* 2012; **154**: 481-494 [PMID: 22167532 DOI: 10.1007/s00701-011-1242-8]
 - 44 **Haacke EM**, Xu Y, Cheng YC, Reichenbach JR. Susceptibility weighted imaging (SWI). *Magn Reson Med* 2004; **52**: 612-618 [PMID: 15334582 DOI: 10.1002/mrm.20198]
 - 45 **Stark DD**, Bradley WG. Magnetic resonance imaging. St. Louis, Missouri: Mosby, 1999; 64
 - 46 **Haneder S**, Attenberger UI, Biffar A, Dietrich O, Fink C, Schoenberg SO, Michaely HJ. Gadofosveset: parameter optimization for steady-state imaging of the thoracic and abdominal vasculature. *Invest Radiol* 2011; **46**: 678-685 [PMID: 21709565 DOI: 10.1097/RLI.0b013e31822428ad]
 - 47 **Cohen J**. A coefficient of agreement for nominal scales. *Educ Psychol Meas* 1960; **20**: 37-46 [DOI: 10.1177/001316446002000104]
 - 48 **Landis JR**, Koch GG. An application of hierarchical kappa-type statistics in the assessment of majority agreement among multiple observers. *Biometrics* 1977; **33**: 363-374 [PMID: 884196]
 - 49 **Landis JR**, Koch GG. The measurement of observer agreement for categorical data. *Biometrics* 1977; **33**: 159-174 [PMID: 843571]
 - 50 **Bushberg JT**. The Essential Physics of Medical Imaging. 2nd ed. Philadelphia: Lippincott Williams and Wilkins, 2006
 - 51 **Østergaard K**, Sunde N, Dupont E. Effects of bilateral stimulation of the subthalamic nucleus in patients with severe Parkinson's disease and motor fluctuations. *Mov Disord* 2002; **17**: 693-700 [PMID: 12210858 DOI: 10.1002/mds.10188]
 - 52 **Kitagawa M**, Murata J, Kikuchi S, Sawamura Y, Saito H, Sasaki H, Tashiro K. Deep brain stimulation of subthalamic area for severe proximal tremor. *Neurology* 2000; **55**: 114-116 [PMID: 10891917]
 - 53 **Cuny E**, Guehl D, Burbaud P, Gross C, Dousset V, Rougier A. Lack of agreement between direct magnetic resonance imaging and statistical determination of a subthalamic target: the

- role of electrophysiological guidance. *J Neurosurg* 2002; **97**: 591-597 [PMID: 12296643 DOI: 10.3171/jns.2002.97.3.0591]
- 54 **Kerl HU**, Gerigk L, Huck S, Al-Zghloul M, Groden C, Nölte IS. Visualisation of the zona incerta for deep brain stimulation at 3.0 Tesla. *Clin Neuroradiol* 2012; **22**: 55-68 [PMID: 22349435 DOI: 10.1007/s00062-012-0136-3]
- 55 **Nakada T**. Clinical application of high and ultra high-field MRI. *Brain Dev* 2007; **29**: 325-335 [PMID: 17113259]
- 56 **Kosta P**, Argyropoulou MI, Markoula S, Konitsiotis S. MRI evaluation of the basal ganglia size and iron content in patients with Parkinson's disease. *J Neurol* 2006; **253**: 26-32 [PMID: 15981079 DOI: 10.1007/s00415-005-0914-9]
- 57 **McNeill A**, Chinnery PF. Neurodegeneration with brain iron accumulation. *Handb Clin Neurol* 2011; **100**: 161-172 [PMID: 21496576]
- 58 **Zhang W**, Sun SG, Jiang YH, Qiao X, Sun X, Wu Y. Determination of brain iron content in patients with Parkinson's disease using magnetic susceptibility imaging. *Neurosci Bull* 2009; **25**: 353-360 [PMID: 19927171]
- 59 **Gelman N**, Gorell JM, Barker PB, Savage RM, Spickler EM, Windham JP, Knight RA. MR imaging of human brain at 3.0 T: preliminary report on transverse relaxation rates and relation to estimated iron content. *Radiology* 1999; **210**: 759-767 [PMID: 10207479]
- 60 **Park JH**, Chung SJ, Lee CS, Jeon SR. Analysis of hemorrhagic risk factors during deep brain stimulation surgery for movement disorders: comparison of the circumferential paired and multiple electrode insertion methods. *Acta Neurochir (Wien)* 2011; **153**: 1573-1578 [PMID: 21476122 DOI: 10.1007/s00701-011-0997-2]
- 61 **Balachandran R**, Welch EB, Dawant BM, Fitzpatrick JM. Effect of MR distortion on targeting for deep-brain stimulation. *IEEE Trans Biomed Eng* 2010; **57**: 1729-1735 [PMID: 20388592 DOI: 10.1109/TBME.2010.2043675]
- 62 **Duchin Y**, Abosch A, Yacoub E, Sapiro G, Harel N. Feasibility of using ultra-high field (7 T) MRI for clinical surgical targeting. *PLoS One* 2012; **7**: e37328 [PMID: 22615980 DOI: 10.1371/journal.pone.0037328]
- 63 **Shmueli K**, de Zwart JA, van Gelderen P, Li TQ, Dodd SJ, Duyn JH. Magnetic susceptibility mapping of brain tissue in vivo using MRI phase data. *Magn Reson Med* 2009; **62**: 1510-1522 [PMID: 19859937 DOI: 10.1002/mrm.22135]

P- Reviewer Antoniou P **S- Editor** Song XX
L- Editor Webster JR **E- Editor** Xiong L

